Recapitulating aortic valve disease hemodynamics with a highly tunable bio-inspired soft robotic aortic sleeve

Luca Rosalia
Massachusetts Institute of Technology https://orcid.org/0000-0002-7214-7859
Caglar Ozturk
Massachusetts Institute of Technology
Yiling Fan
Massachusetts Institute of Technology
Jaume Coll-Font
A.A. Martinos Center for Biomedical Imaging
Shi Chen
A.A. Martinos Center for Biomedical Imaging
Robert Eder
A.A. Martinos Center for Biomedical Imaging
Jo Kim
A.A. Martinos Center for Biomedical Imaging
Yasufumi Nagata
Massachusetts General Hospital
Robert Levine
Massachusetts General Hospital
Marcello Panagia
Boston University Medical Center
Jose Guerrero
Massachusetts General Hospital
Adam Mauskapf
Massachusetts General Hospital
Ellen Roche
Massachusetts Institute of Technology https://orcid.org/0000-0002-8952-2993
Christopher Nguyen (Christopher.Nguyen@mgh.harvard.edu)
Massachusetts General Hospital / Harvard Medical School https://orcid.org/0000-0003-1475-2329

Article

Keywords: aortic stenosis (AS), aortic sleeve, aortic valve disease

Posted Date: July 22nd, 2021

DOI: https://doi.org/10.21203/rs.3.rs-713582/v1

Version of Record: A version of this preprint was published at Nature Biomedical Engineering on September 26th, 2022. See the published version at https://doi.org/10.1038/s41551-022-00937-8.

Abstract

Existing models of aortic stenosis (AS) are limited to inducing left ventricular pressure overload. As they have reduced control over the severity of aortic constriction, the clinical relevance of these models is largely hindered by their inability to mimic AS hemodynamics and recapitulate flow patterns associated with congenital valve defects, responsible for the accelerated onset and progression of AS. Here we report the development of a highly tunable bio-inspired soft robotic tool that enables the recapitulation of AS in a porcine model, in which customization of actuation patterns allows hemodynamic mimicry of AS and congenital aortic valve defects. *In vitro* and computational tools including lumped-parameter, finite element, and computational fluid dynamics platforms were developed to predict the hemodynamics induced by the bio-inspired soft robotic sleeve. The controllability of our *in vivo* model and its ability to replicate flow patterns of AS and congenital defects were demonstrated in swine through echocardiography, left ventricular catheterization, and magnetic resonance imaging. This work supports the use of soft robotics to simulate human physiology and disease, while paving the way towards the development of patient-specific models of AS and congenital defects that can guide clinical decisions to improve the management and treatment of these patients.

Introduction

Advances in soft robotics have led to the development of high-fidelity simulators of pathophysiology for biomedical applications[1]. By utilizing materials with mechanical properties similar to those of biological tissues, soft robots are capable of recapitulating the biomechanical function and complex motion dynamics of various organ systems, including the heart[2], the gastrointestinal tract[3,4], the respiratory system[5,6] and others[7,8]. These simulators could serve as platforms for testing and development of medical therapies, as well as studies of human physiology and disease. However, they can only model organ systems in isolation, failing to capture the complex physiologic interplay arising for example from neurohormonal control and feedback or compensation mechanisms. Here, we present an *in vivo* disease model that utilizes a bio-inspired soft robotic sleeve to recapitulate the hemodynamics of aortic stenosis (AS) and congenital aortic valve defects in swine, and describe the use of computational tools and 4D magnetic resonance imaging (MRI), among other techniques, to ensure faithful hemodynamic mimicry.

The prevalence of AS is rising in the U.S., with more than 1.5 million Americans being diagnosed every year[9]. AS is an obstruction of blood flow through the aortic valve mediated by calcification and inflammatory processes, often accelerated by congenital aortic valve defects[9–11]. If untreated, AS can result in heart failure[11–14] and sudden death[15]. High-fidelity *in vivo* models of AS may advance the development of risk stratification frameworks to guide the management of AS, and particularly of asymptomatic cases of severe AS for whom interventional guidelines remain heterogeneous[11,16]. Further, these models may help elucidate why, despite the elevated overall success rates of aortic valve replacement, repeat procedures and perioperative mortality rates remain high in certain patient groups[17,18].

The majority of former *in vivo* models of AS utilize rigid bands or inflatable cuffs around the ascending aorta to induce left ventricular (LV) pressure overload[19–21]. These devices can only achieve concentric constriction of the aorta, and fail to recreate the complex 3D flow patterns observed in AS. Moreover, their limited control prevents them from recapitulating the hemodynamics of congenital aortic valve defects – often accelerating the onset and progression of AS, as well as aortic remodeling, potentially leading to other complications including aortic aneurysms, dissection, and regurgitation[22]. Bicuspid aortic valve (BAV) disease is the most common congenital valve disease. In this work, we specifically focus on bicommissural bicuspid valves (henceforth simply referred to as bicommissural)[11,23,24]. Another disease phenotype is unicommissural aortic valve (UAV). UAV is more rare and associated with an even poorer prognosis than BAV, albeit depending on the morphology of the defect[25–27].

Here, we report the development of a highly tunable bio-inspired soft robotic aortic sleeve that recapitulates the hemodynamics of AS and of congenital valvular defects – unicommissural or bicommissural (Fig. 1). With the potential to recreate patient-specific hemodynamic profiles, this research pioneers the development of high-fidelity, customizable *in vivo* models of human disease. This bio-inspired soft robotic technology is poised to model a broader spectrum of human diseases, paving the way towards other medical applications including studies of vascular (e.g., carotid, peripheral arterial disease, aortic coarctation) or pulmonary valve stenosis, urinary or gastrointestinal sphincter dysfunction, and airway obstruction. These models could therefore provide insights into a wide range of pathophysiological conditions and support translational research by guiding innovation in medical devices and therapies.

Results

Design and development of a highly tunable bio-inspired soft robotic aortic sleeve

A highly tunable bio-inspired soft robotic aortic sleeve was developed to recapitulate the hemodynamics of AS and congenital aortic valve disease. This is composed of three expandable elements or pockets, each connected to one hydraulic line for actuation, where activation of one pocket mimics fusion or stiffening of one corresponding commissure – the area where the valve leaflets abut. An inelastic fabric sheet spanning across the base of the soft actuator restrains the expansion of the pockets to one direction under hydraulic pressure and a slit and strip mechanism allows positioning around the outer wall of the porcine aorta.

The expandable bladder is made of two vacuum formed sheets of Thermoplastic Polyurethane (TPU), whereas a TPU-coated Nylon fabric is used as the constraining layer. A positive and a negative mold of the bladder were made for vacuum forming and sealing of the expandable elements respectively (Fig. 2a-b) (see Methods). Figure 2c illustrates the mechanical response to uniaxial loading of the TPU and Nylon layers, and the axial force generated by the sleeve versus actuation volume is depicted in Fig. 2d (see Methods). 3D representations of the sleeve with details of the pockets, the constraining layer, the positioning mechanism, and the actuation lines are shown in Fig. 2e-f. Histology studies on each of the

materials constituting the aortic sleeve resulted in minimal fibrous tissue and no significant lymphocytic infiltrates (see Methods and Supplementary Information).

This highly tunable bio-inspired soft robotic sleeve was designed to recapitulate the hemodynamics of AS and of congenital defects, namely of unicommissural and bicommissural aortic valves.

Selective pocket actuation enables customization of aortic luminal geometries for hemodynamic mimicry of aortic valve defects: in vitro **and finite element studies**

A simple mock circulatory loop (MCL) and a finite element (FE) simulation were developed to predict the structural response of the ascending aorta upon activation of the sleeve. A schematic representation of the main elements constituting the MCL, including a mock aortic vessel with a modulus matched with native aortic tissue for placement of the sleeve, is provided in Fig. 3a. Changes in the luminal cross-section of the aorta are visualized using an endoscopic camera inserted in the MCL. Figure 3b illustrates an accurate 3D representation of the sleeve placed around the ascending aorta of the Living Heart Model on Abaqus 2018 (Dassault Systèmes, Simulia)[28,29] for the FE study. Details of the MCL and FE simulation set-up can be found in the Methods.

Selective activation of the pockets of the aortic sleeve results in various constriction profiles, where each actuated pocket mimics the hemodynamics associated with a fused commissure of the aortic valve (Fig. 3c-e). Specifically, a bicommissural profile is obtained from actuation of one pocket (Fig. 3c), a unicommissural geometry is achieved when two pockets are activated (Fig. 3d), while actuation of all the three pockets results in partial fusion of the three commissures, leading to a stenotic profile (Fig. 3e).

Following the same pocket actuation schemes, structural FE characterization of the ascending aorta show analogous findings to those obtained in the MCL study. Figure 3c-e illustrates the cross-sectional profiles obtained via FE, further corroborating the ability of the sleeve to recapitulate bicommissural, unicommissural and stenotic aortic geometries.

Lumped-parameter *in silico* model predicts the hemodynamics of aortic constriction

A lumped-parameter (LP) model previously developed by our group[30,31] was adapted to the porcine physiology to simulate the hemodynamics of aortic constriction. The domain (Fig. 4a) is composed of a four-chamber heart, proximal vasculature, and lumped-parameter elements modeling the peripheral and pulmonary circulations. Constrictions of the ascending aorta were simulated as reductions in the luminal cross-sectional area of the *Band* element (see Methods). Left ventricular (LV) pressure-volume (PV) loops were obtained at baseline and at *Intermediate* (80%) and *Full* (90%) constrictions (Fig. 4b), and metrics of cardiac function such as arterial elastance (Ea), peak LV pressure (LVP) and stroke volume (SV) were extracted (Fig. 4c-e). Further, the maximum transaortic pressure gradient (Fig. 4f) was computed for cross-validation with the MCL *in vitro* system (Fig. 4g).

Figure 4b shows that aortic constriction results in elevated LVP and a drop in the volume of blood ejected during each heart cycle – the stroke volume (SV). This occurs because aortic constriction intrinsically increases the afterload, i.e., the pressure against which the heart has to eject blood during systole, which is reflected in the surge in Ea (2.0 to 22.0 mmHg/mL), as shown in Fig. 4c. Correspondingly, the peak LVP increases from baseline values of 93.2 to 166.6 mmHg, and the SV drops from 40.3 to 7.0 mL. While the peak LVP rises in an approximately linear fashion, the SV decreases more significantly at elevated degrees of aortic constriction.

The maximum transaortic gradient increases exponentially with aortic constriction both according to the LP and the MCL *in vitro* models. Results show that the transaortic pressure gradient begins to rise significantly from values of aortic constriction of approximately 70%. At 80% aortic constriction, gradients of 46.9 mmHg and 45.5 ± 2.3 mmHg were obtained on the LP and MCL platforms respectively, these increasing to 94.0 mmHg and 85.6 ± 7.5 mmHg at 90% constriction (Fig. 4g). Clinically, gradients between 40–65 mmHg correspond to moderate cases of AS, whereas gradients greater than 65 mmHg are indicative of severe AS[32,33]. Overall, these findings suggest that the proposed sleeve is capable of accurately recreating clinically relevant hemodynamics of AS.

Study Design And Overview

The aortic sleeve was implanted in 6 Yorkshire pigs (~ 38-45kg). The timeline of the investigation is shown in Fig. 5. Cardiac function was assessed at the beginning of the study on transthoracic echocardiography (TTE) prior to implantation on day 0 (D0). MRI was performed on D6 to evaluate cardiac function and visualize aortic flow hemodynamics acutely at progressive levels of constriction and following pocket-selective actuation to recreate the bicommissural, unicommissural, and aortic stenosis profiles observed *in vitro* and predicted *in silico*. Acute changes in cardiac function and aortic hemodynamics were re-evaluated before sacrifice eight days post implantation (D8) through transapical LV catheterization and transepicardial echocardiography. During this study, a flow probe was inserted on the thoracic aorta to record changes in blood flow. Findings from these studies were used to validate the FE and LP platforms, as well as the computational fluid dynamics (CFD) model described later in this work.

The effects of various degrees of aortic constriction were evaluated in the aortic stenosis configuration. Further, pocket-specific actuation was performed to recreate bicommissural and unicommissural aortic constriction profiles as previously described. Due to the prolonged time required for MRI image acquisition and associated risks, we limited the severity of aortic constriction during MRI studies.

Through this investigation, one swine was euthanized due to severe cardiac effusion findings on MRI, while two trials were excluded from the analysis due to unsuccessful tensioning of the sleeve during implantation. We report the role of tensioning during implantation of the sleeve and its effect on the degree of constriction in the Supplementary Information. All animal procedures were approved by the Institutional Animal Care and Use Committee (IACUC) of our institute (see Methods).

Highly controllable aortic constriction and *in vivo* hemodynamics

The hemodynamics induced acutely by actuation of the bio-inspired soft robotic aortic sleeve were measured in swine at day 8 (D8). The sleeve was actuated continuously to two degrees of aortic constriction, namely *Intermediate* and *Full*, with up to 3 mL and 4.75 mL of volume deployed respectively. Figure 6a-c shows color map images of blood flow through the aortic valve orifice during ejection on transepicardial echocardiography at baseline (Fig. 6a), and intermediate (Fig. 6b) and full (Fig. 6c) actuation, the latter resulting in mostly complete obstruction of blood flow. Measurements of the corresponding peak aortic flow velocity and estimates of the transaortic pressure gradient (Fig. 6d) yielded peak flow velocities values up to 4.85 ± 0.14 m/s and pressure gradients of 94.13 ± 5.49 mmHg, corresponding to severe clinical cases of AS[32,33]. Analysis of LV systolic function through measurements of left ventricular ejection fraction (LVEF) showed a progressive drop at intermediate (31.5 ± 2.8 %) and full (10.9 ± 4.2 %) constriction, while comparison between baseline at D8 (50.3 ± 2.7 %) and D0 (55.8 ± 4.0 %) revealed no remarkable changes induced by sole implantation of the sleeve prior to actuation (Fig. 6e). Correspondingly, mean blood flow at the thoracic aorta dropped 5-fold from baseline values of 2.60 ± 0.23 L/min to 0.52 ± 0.14 L/min at full constriction (Fig. 6f).

Results from LV catheterization with a PV catheter (Fig. 6g-j) show similar trends as those predicted by the LP model, with a sharp increase in Ea (1.86 ± 0.18 to 24.24 ± 3.13 mmHg/mL) (Fig. 6h), an approximately linear rise in peak LVP (90.31 ± 9.45 to 164.89 ± 9.49 mmHg) (Fig. 6i) and a drop in SV (44.02 ± 2.9 to 6.23 ± 1.00 mL), which becomes increasingly significant at more severe degrees of aortic constriction (Fig. 6j). Notably, these changes are statistically significant for both degrees of aortic constriction and in close agreement with the *in silico* model. Details of the techniques used for hemodynamic assessment, and a summary of the data and statistical analysis can be found in the Methods and Supplementary Information.

Discussion

High-fidelity models of human physiology and disease are poised to have important implications in human health and clinical medicine. Soft robotic technology has enhanced the accuracy of benchtop or biohybrid simulators that can recapitulate the biomechanics and function of a variety of organ systems[1]. Although animal models of human disease are not as broadly documented in the scientific literature, attempts have been made to induce pressure overload secondary to aortic stenosis (AS) – one of the most highly prevalent valvular heart diseases[19,21,34]. However, existing technologies only enable concentric aortic constriction of the aorta, thus failing to recreate the complex aortic flow hemodynamics associated with AS. Further, they suffer from limited controllability, elevated mortality rates, and the inability to recapitulate the hemodynamics of congenital valve defects, which often accelerate symptoms of AS, emphasizing the need for more comprehensive and representative models of this condition.

In this work, we described the development of a high-fidelity *in vivo* model of AS by means of a bio-inspired soft robotic aortic sleeve. This is composed of expandable elements or pockets that can be

individually activated to enable customization of aortic flow patterns. A broad array of computational tools, including lumped-parameter (LP), finite element (FE) and computational fluid dynamic (CFD) platforms were developed to predict the structural and hemodynamic effects induced by the aortic sleeve, then validated *in vivo*. Specifically, echocardiography, and LV catheterization were leveraged to evaluate cardiac function and aortic hemodynamics, whereas 4D-MRI enabled visualization of aortic flow patterns and comparison with CFD modeling.

This *in vivo* disease model can simulate abnormalities in peak aortic flow velocity, transaortic pressure gradient, and LV hemodynamics in a controllable way. Intermediate and full activation of the aortic sleeve yielded significant differences in aortic flow, and metrics of left ventricular ejection fraction (LVEF), arterial elastance (Ea), peak left ventricular pressure (LVP) and stroke volume (SV). Notably, the changes induced upon constriction were seen to correspond to clinical cases of AS according to the American Society of Echocardiography (ASE) and the European Association of Cardiovascular Imaging (EACVI)[33]. In addition to approximating clinically relevant metrics for AS assessment, this model was shown to recreate bicommissural, unicommissural, and stenosis geometries and hemodynamics similar to those associated with congenital valve defects or calcific AS.

The enhanced control provided by this bio-inspired soft robotic aortic sleeve could enable patient-specific studies of pressure overload secondary to AS, supporting the development of interventions for AS and of hemodynamics-based algorithms for clinical decision making. Chronically, AS may lead concentric remodeling and symptoms of heart failure with preserved ejection fraction (HFpEF)[14,35]. Further, depressed contractility and heart failure with reduced ejection fraction (HFrEF) may ensue in severe cases of AS when cardiac compensation is inadequate[36]. By enabling recapitulation of patient-specific hemodynamics, this work could allow hemodynamically accurate studies of the progression of heart failure secondary to AS, closely mimicking the pathophysiology of chronic disease and overcoming the limitations of existing models, such as reduced controllability and elevated mortality rates. In addition, reversing the degree of aortic constriction in a controlled way could help explore the efficacy of aortic valve replacement procedures in ameliorating adverse remodeling, and investigate the onset of plasticity during these processes, following which hemodynamic and pathophysiological derangements cannot be fully overturned[37,38].

Congenital valve defects lead to a dramatic acceleration in the progression of AS and associated symptomatology[23,25,27]. While *ex vivo* models of congenital valve disease have been recently developed[39], in this work, we have recreated the hemodynamics of bicommissural and unicommissural congenital defects as well as calcific AS, using a combination of *in silico, in vitro* and *in vivo* techniques. The ability of this bio-inspired soft robotic sleeve to be programmed and reconfigured to different constriction profiles over time makes it ideal for long-term studies of aortic constriction and congenital defects.

Feeding *in vivo* data into the proposed computational platforms could enhance their physiologic relevance. These *in silico* tools could be optimized to customize the design of the sleeve and actuation

patterns to closely approximate patient-specific flow profiles. This would enable the development of patient-specific *in vivo* models of disease, which could provide a holistic view of the relevant pathophysiology and better inform prognosis and treatment strategies.

This research pioneers the development of high-fidelity *in vivo* models of human disease by leveraging soft robotics technology and advances in MRI for hemodynamic mimicry and with potential for patient-specific applications. It could inspire *in vivo* models of other pathophysiological conditions, within and beyond the cardiovascular field. For example, the design of the aortic sleeve could be modified to enable studies of pulmonary hypertension and right heart failure where flow patterns across the pulmonary valve can be accurately recreated. Other examples may involve studies of esophageal and swallowing disorders, including abnormal peristalsis, spasms, and of the aerodynamics of airway obstructions for a variety of respiratory or other biomedical applications.

Methods

Bio-inspired soft robotic aortic sleeve manufacture

Each soft actuator is manufactured by first vacuum forming two sheets of Thermoplastic Polyurethane (TPU) into a 3D-printed mold. A 1mm diameter opening is created in the geometrical center of each of the three pockets of one of the two sheets, where half of a PVC is then inserted. The two TPU sheets are then heat-sealed at a temperature of 320F for 10 seconds. The same heat-sealing procedure is then repeated to attach the bottom side of the TPU bladder (i.e., where the PVC connectors are inserted) to the coated inelastic fabric which has three openings corresponding to the TPU connectors. Soft tubing is then secured to each of the connectors to enable independent activation of each of the three pockets of the actuator. The fabric is then cut to shape to create a slit along its short side and a strip on its long axis for positioning around the aorta. A detailed description of the manufacturing process and the materials used can be found in the Supplementary Information.

Mechanical characterization

The modulus of elasticity (E-modulus) of the TPU and fabric layers was determined under uniaxial tensile loading using an electromechanical tester (Instron 5566, 2kN load cell, Norwood, USA), according to the ISO 527-1 and ISO 13934-1 standards for plastics and textiles respectively. The E-modulus was calculated as the slope of the stress-strain curve at 0–5% elongation.

The axial force exerted by the actuator at inflation was measured on the same instrument. The lower plate of the electromechanical tester served as an attachment point for the aortic sleeve, whereas the upper one was connected to the load cell and brought in close contact with the upper surface of the actuator. The sleeve was actuated by deploying up to 5mL of saline using a syringe pump (70-3007 PHD ULTRA™ Syringe Pump Infuse/Withdraw, Harvard Apparatus) continuously at a rate of 0.2 mL/sec, and the applied force was measured by the load cell. Each of these mechanical tests was conducted on three samples (n = 3). Average values and SD were calculated.

Mock circulatory loop (MCL)

A simple mock circulatory loop (MCL) was built utilizing a pulsatile pump (55-3305 Pulsatile Blood Pump, Harvard Apparatus), two adjustable compliance chambers and resistive valves in series, and a low-modulus latex tubing ($E \approx 1.4$ MPa, d_{in} = 1/2”, d_{out} = 5/8”, McMaster-Carr) to approximate the elasticity and geometry of the porcine ascending aorta. Pressure sensors (Wireless Pressure Sensor PS-3203, PASCO) enabled pressure measurements across the mock vessel. An endoscopic camera (1080P HD, 30 fps, NIDAGE) was inserted in the MCL to visualize the cross-section of the aorta. The stroke volume and the rate of the pulsatile pump were manually adjusted to values of 30 mL and 100 bpm. The soft robotic actuator was secured around the mock vessel. Activation was performed by deploying up to 6 mL of saline through a syringe pump as described in the *Mechanical characterization* Methods section above. The pressure across the aorta was continuously recorded and displayed in real-time on the PASCO Capstone 2.2.0 software (PASCO) throughout actuation. The maximum transaortic pressure gradient was calculated, whilst synchronous images of the luminal cross-section of the aorta were processed on the Image Labeler Application of the MATLAB Image Processing and Computer Vision toolbox (MathWorks®) to estimate the luminal aortic cross-sectional area.

Lumped-parameter (LP) modeling

A lumped-parameter model was constructed on the MATLAB-based object-oriented environment SIMSCAPE FLUIDS™ (MathWorks®), based on our previous work[30,31]. The geometrical dimensions of the heart chambers, heart valves, and proximal vasculature were defined using CINE MRI, while other lumped-parameter resistive and capacitive elements were adapted from our previous work to approximate the porcine hemodynamics measured through LV catheterization *in vivo*. A summary of the input parameters and of the simulated hemodynamics at baseline and comparison with *in vivo* data can be found in the Supplementary Information. Aortic constriction (AC) was simulated by reducing the luminal cross-sectional area of the *Band* element (Fig. 3a) by 10–90% in 10%-step increments. PV loops were obtained for values of aortic constriction equal to 80% (intermediate) and 90% (full).

Finite element (FE) modeling

Finite element analysis (FEA) was conducted to evaluate the biomechanical effects of the soft robotic sleeve on the ascending aorta. The heart model was adapted from the Living Heart Model (LHM)[29] and used on Abaqus 2018 software (Simulia, Dassault Systèmes). The LHM represents a well-defined human anatomy, including four dynamic ventricles, aorta (ascending and aortic arch), atria and pulmonary artery based on cardiac MRI data[28]. To simulate aortic constriction in a swine model, the aortic arch was scaled down to approximate in vivo measurements (ID ~ 19mm, OD ~ 20mm).

Nonlinear explicit dynamic analysis was performed to simulate the constriction profiles and the deformation of aorta. An accurate 3D representation of the band was constructed in SOLIDWORKS (Dassault Systèmes, 2019) and imported into the FEA model. The sleeve pockets were modeled as 3-node triangular shell elements (S3R) and assigned Neo-Hookean hyperelastic TPU material properties. Uniaxial test data (Fig. 2c) was used as an input source for the hyperelastic model. The aorta was modeled using an anisotropic hyperelastic material model for cardiac tissue[29]. Further details regarding the LHM can be

found in previous studies[28,29,40]. Surface-based fluid cavities were defined to represent the fluid inside the actuator pockets and the ascending aorta. The hydrostatic fluid elements inside the surfaces govern the relationship between mechanical deformation, cavity pressure and volume, hence predict the mechanical response of fluid-filled structures.

The FEA simulation consisted of two steps. In the first step, the pockets were depressurized to achieve a deflated shape, and the aortic pressure was increased to 100 mmHg. In the next and final step, the pockets were gradually pressurized to achieve full aortic constriction. These studies were performed using Abaqus/Explicit solver and were completed in approximately 3 hours on a desktop PC with a 3.0 GHZ i7-9700 processor with 8 cores and 32 GB RAM.

Computational fluid dynamic (CFD) modeling

In this study, a Large-Eddy Simulation (LES) turbulence model was utilized in XFlow 2020 software (Dassault Systèmes) using a particle-based and fully Lagrangian approach to model aortic flow patterns. Blood was modeled as an incompressible Newtonian fluid and turbulence was simulated using the Wall-Adapting Local Eddy viscosity model[41,42]. The deformed structure of the ascending aorta was imported into the XFlow domain for each actuation profile. The inlet surface of the ascending aorta was extended to facilitate convergence. Further details regarding the definition of the inlet and outlet boundary conditions can be found in the Supplementary Information.

The wall surface was assumed to be rigid, and the no-slip condition was applied. The total simulation time was set to 1.45 seconds (~ 2 cycles) and the time step $\Delta t = 1x10^{-5}s$ was applied for each simulation to ensure numerical stability. Grid independency was achieved at 0.8 mm resolution with approximately 159,000 elements. The refinement method with 0.2 mm resolution was applied near the walls to ensure a sufficient amount of lattice elements at the constriction region as a boundary layer. Analysis was completed in ~ 6 hours on a desktop PC with a 3.0 GHZ i7-9700 processor with 8 cores and 32 GB RAM.

Histology studies

Each of the materials constituting the aortic sleeve presented in this work was implanted subcutaneously in one Sprague Dawley rat to investigate the response of the surrounding tissue 28 days post-implantation. Four subcutaneous pockets were created surgically on the back of the rat to enable placement of the materials. The samples implanted were as follows: the TPU sheet constituting the expandable elements of the sleeve; the TPU-coated fabric used as the inelastic constraining layer of the sleeve; a short segment of the actuation line made of Polyurethane, and a Polycarbonate connector. Images of the digitized slides can be found in Supplementary Information, as well as further details regarding animal handling and the implantation procedure.

Animal preparation

In vivo studies were conducted on a total of 6 Yorkshire swine (~ 38-45kg) housed in the Massachusetts General Hospital Center for Comparative Medicine Large Animal Facility. The swine were kept under 12-h

light/12-h dark cycles with access to a standard diet of food and water *ad libitum*. Starting 72h prior to the implantation procedure, animals were given oral amiodarone. Before the procedure, animals were anesthetized, intubated with an endotracheal tube and placed on a ventilator with isoflurane and oxygen. Immediately prior to the procedure, animals received an intramuscular injection of buprenorphine, carprofen and a continuous infusion of fentanyl citrate. The swine were administered cefazolin, and a constant infusion of amiodarone and 2% Lidocaine for the duration of the procedure.

Implantation of the aortic band involved a thoracotomy with incisions at the level of the fourth intercostal space. Muscles layers were separated through blunt dissection to access the thoracic cavity and the ascending aorta. The sleeve was wrapped around the ascending aorta, pre-tensioned by pulling the strip through the slit, and then secured using sutures. Pre-tensioning was considered successful when the strip could be pulled entirely through the slit and when no space between the sleeve and the porcine aorta could be noticed upon visual and tactile inspection. Due to anatomical variations, adequate pre-tensioning could not be achieved in 2 of the 6 pigs, which were therefore discarded from the analysis. Details of the effects of pre-tensioning on the hemodynamics of aortic constriction can be found in the Supplementary Information.

Following successful implantation, the apical suture and retractor were removed. The lungs were over-inflated for 3–4 breaths to evacuate excess fluid and prevent pneumothorax. The cavity and skin could then be closed via suturing in a layer-by-layer fashion. The lines from the sleeve remained external to the animal. Postoperative analgesia was provided with a transdermal fentanyl path and oral carprofen. Oral antibiotics were administered 72h post operation.

Prior to the MRI study (D6), the animals were administered anesthesia and intubated. Body temperature was supported using a circulating water heat pad placed between the animal and the MRI table. A pulse oximeter, blood pressure cuff and spirometer were all placed to monitor the animals' vitals throughout scanning procedures. MRI revealed significant pericardial effusion of one animal, which was therefore euthanized prior to conducting any aortic constriction procedures. Following successful MRI, animals were recovered and monitored.

Before terminal hemodynamic evaluation (D8), the swine were placed under anesthesia following the same regiment as described above. After echocardiography, LV catheterization, and thoracic aortic flow measurements, animals were euthanized with saturated potassium chloride. Changes in the animal's heart rate and blood pressure due to anesthesia were monitored. More details on the animal procedure and drug dosages can be found in the Supplementary Information.

Echocardiography

LV systolic function and flow profile across the proximal ascending aorta were evaluated using a commercial ultrasound system (IE33/X5-1 or X7-2 transducer, Philips, Andover, MA) at D0 (transthoracic) and at D8 (transepicardial). M-mode echocardiography on the LV in short axis view and continuous pulse-Doppler echocardiography across the proximal ascending aorta in an apical view were recorded during continuous activation of the aortic sleeve to evaluate changes in the LV function and the flow profile due

to aortic constriction[43]. Acquired echocardiographic data were analyzed with syngo Dynamics (Siemens Healthineers, Erlangen, Germany). From measurements of the LV end-diastolic and -systolic diameters, LV volumes and ejection fraction were estimated with the Teichholz method[44].

Peak pressure gradient ΔP was calculated from measured values of the peak outflow velocity v_{max} by the simplified Bernoulli equation[33] (equation 1):

$$\Delta P = 4\, v_{max}^2 \qquad (1)$$

Echocardiographic studies were conducted on n = 2 swine, as these procedures were included in the protocol only at a later stage.

Magnetic resonance imaging

Each animal was scanned one of two 3T clinical MRI systems (Biograph mMR scanner, 45mT/m gradient system and a MAGNETOM Prisma, 80mT/m gradient system, Siemens Healthineers, Erlangen, Germany), both equipped with a standard 32-channel antero-posterior surface coil. Animals were imaged with a whole heart CINE MRI as well as 2D/4D cardiac flow MRI sequences centered on the aortic constriction. Whole heart CINE MRI acquisitions were performed with a balanced steady-state free precession (bSSFP) sequence along the short axis plane with the following parameters (resolution 1.4x1.4x6.0 mm^3, matrix size 128/85, 10/15 slices depending on the heart size, pixel bandwidth (BW) 1500 Hz/pixel, echo time (TE) 2.79 ms, repetition time (TR) 30.72 ms and retrospective ECG gating with 25 segments). The aortic flow sequence was done with a 2D or 3D gradient echo (GRE) sequence depending on the scanner utilized.

On the Biograph mMR scanner, 2D flow was acquired with velocity encoding along the through-plane direction and images obtained in the short axis plane centered on the aortic band. The sequence parameters for the 2D flow were the following: velocity encoding (VENC) 500 mm/s, resolution 1.4x1.4x6.0 mm^3, matrix size 256x152 and 12 to 15 slices, BW 490 Hz/pixel, TE/TR 3.41/23.52 ms and retrospective ECG gating over 23 segments.

On the MAGNETOM Prisma scanner, the 4D flow sequence was acquired with velocity encoding along the through-plane direction, left/right and head/feet directions and images obtained in the short axis plane centered on the aortic band. The sequence parameters were the following: velocity encoding (VENC) 500 mm/s, resolution 1.4x1.4x2.5 mm^3, matrix size 208x166 and 28 slices to cover the entire aortic arch, BW 490 Hz/pixel, TE/TR 2.07/15.6 ms, retrospective ECG gating over 27 segments and respiratory gating with a pencil beam navigator placed on the liver dome and acceptance window of 8mm.

Details on the reconstruction of the LV geometries, 4D flow analysis and estimates of LVEF on MRI can be found in the Supplementary Information.

Left ventricle catheterization

In vivo LV PV data were collected using the Transonic ADV500 PV System and the 5F straight tip PV loop catheter (Transonic Systems, Inc., Ithaca, NY). The catheter was inserted transapically during the open-chest surgery. Through real-time pressure measurements, the catheter was guided through the aortic

valve and gradually retrack back to the LV to ensure consistent catheter positioning. The catheter was then rotated to minimize the interference with mitral-valve and/or papillary muscle. Data were collected with 400 Hz sampling rate with a 50 Hz low-pass filter applied to the volume data.

Thoracic aorta flow

Flow at the thoracic aorta was measured using the TS420 Perivascular Flowmeter Module with the MA-12PAU flow probe (Transonic Systems, Inc., Ithaca, NY). Data were collected under low range setup (0 ~ 1.2 Volt) with a 10 Hz filter. Flow rate was estimated using the pre-calibrated unit conversion factor (25mL/min/V).

Data processing and visualization

MATLAB® R2020a (MathWorks®) was used for data processing and visualization. One-way analysis of variance (ANOVA) was performed to determine significance across groups. Data are shown as mean ± SD across trials. When present, smaller error bars indicate the SD of three representative consecutive heart cycles within one trial. The number of heart cycles was kept at a minimum to minimize the risks associated with prolonged full constriction, i.e., when blood flow at ejection is almost entirely blocked by the soft robotic sleeve. For consistency, three representative heart cycles were also averaged for measurements at baseline and intermediate constriction. Details on statistical significance are provided in the Supplementary Information.

Declarations

Data availability

Data (mean +/- standard deviation) for each trial and associated statistics are available in the Supplementary File. The raw dataset used in this study is large and available upon request.

Code availability

Codes used for modelling, and data acquisition, processing, and analysis are available upon request.

Acknowledgements

The authors acknowledge funding from the Harvard-Massachusetts Institute of Technology Health Sciences and Technology program, the SITA Foundation Award from the Institute for Medical Engineering and Science, the MathWorks Engineering Fellowship Fund, the Hassenfeld Research Scholar, the Massachusetts General Hospital SPARK Award, and grants R01HL151704, R01HL135242, and R01HL159010.

Author contributions

L.R., C.O., RA. L., M.P., ET.R., CT.N. planned the study and designed the experiments. L.R., ET.R., CT.N. wrote the manuscript. L.R., C.O designed the device, conducted *in vitro* testing, and developed the *in silico*

models. L.R., C.O., Y.F., J.F-C, Y.N. conducted *in vivo* testing. L.R., S.C., R.E., J.K. provided support for all animal handling procedures. A.M., JL. G. performed animal surgeries.

Competing interests

The authors declare no competing interests.

References

1. Maglio, S., Park, C., Tognarelli, S., Menciassi, A. & Roche, E. T. High-Fidelity Physical Organ Simulators: From Artificial to Bio-Hybrid Solutions. *IEEE Trans. Med. Robot. Bionics* **3**, 349–361 (2021).

2. Park, C. *et al.* An organosynthetic dynamic heart model with enhanced biomimicry guided by cardiac diffusion tensor imaging. *Sci. Robot.* **5**, (2020).

3. Bhattacharya, D., J.V. Ali, S., Cheng, L. K. & Xu, W. RoSE: A Robotic Soft Esophagus for Endoprosthetic Stent Testing. *Soft Robot.* (2020) doi:10.1089/soro.2019.0205.

4. Dang, Y. *et al.* SoGut: A Soft Robotic Gastric Simulator. *Soft Robot.* (2020) doi:10.1089/soro.2019.0136.

5. Ranunkel, O., Güder, F. & Arora, H. Soft Robotic Surrogate Lung. *ACS Appl. Bio Mater.* **2**, 1490–1497 (2019).

6. Horvath, M. A. *et al.* An organosynthetic soft robotic respiratory simulator. *APL Bioeng.* **4**, (2020).

7. Lu, X., Xu, W. & Li, X. A Soft Robotic Tongue-Mechatronic Design and Surface Reconstruction. *IEEE/ASME Trans. Mechatronics* **22**, 2102–2110 (2017).

8. Horvath, M. A. *et al.* Design and Fabrication of a Biomimetic Circulatory Simulator with Overlaid Flow and Respiration Mechanism for Single Ventricle Physiology. in *Proceedings of the IEEE RAS and EMBS International Conference on Biomedical Robotics and Biomechatronics* vols 2020-Novem 74–79 (2020).

9. Nkomo, V. T. *et al.* Burden of valvular heart diseases: a population-based study. *Lancet* **368**, 1005–1011 (2006).

10. Mrsic, Z., Hopkins, S. P., Antevil, J. L. & Mullenix, P. S. Valvular Heart Disease. *Primary Care - Clinics in Office Practice* vol. 45 81–94 (2018).

11. Carabello, B. A. & Paulus, W. J. Aortic stenosis. *The Lancet* vol. 373 956–966 (2009).

12. Grossman, W., Jones, D. & McLaurin, L. P. Wall stress and patterns of hypertrophy in the human left ventricle. *J. Clin. Invest.* **56**, 56–64 (1975).

13. Borlaug, B. A. & Paulus, W. J. Heart failure with preserved ejection fraction: Pathophysiology, diagnosis, and treatment. *Eur. Heart J.* **32**, 670–679 (2011).

14. Borlaug, B. A. Evaluation and management of heart failure with preserved ejection fraction. *Nat. Rev. Cardiol.* **17**, 559–573 (2020).

15. Taniguchi, T. *et al.* Sudden death in patients with Severe Aortic Stenosis: Observations from the CURRENT AS registry. *J. Am. Heart Assoc.* **7**, (2018).

16. Otto, C. M. *et al.* 2020 ACC/AHA Guideline for the Management of Patients With Valvular Heart Disease: A Report of the American College of Cardiology/American Heart Association Joint Committee on Clinical Practice Guidelines. *Circulation* **143**, e72–e227 (2021).

17. Brennan, J. M. *et al.* Long-term survival after aortic valve replacement among high-risk elderly patients in the United States: Insights from the society of thoracic surgeons adult cardiac surgery database, 1991 to 2007. *Circulation* vol. 126 1621–1629 (2012).

18. Jones, J. M. *et al.* Repeat heart valve surgery: Risk factors for operative mortality. *J. Thorac. Cardiovasc. Surg.* **122**, 913–918 (2001).

19. Yarbrough, W. M. *et al.* Progressive induction of left ventricular pressure overload in a large animal model elicits myocardial remodelling and a unique matrix signature. *J. Thorac. Cardiovasc. Surg.* **143**, 215–223 (2012).

20. Olver, T. D. *et al.* Western Diet-Fed, Aortic-Banded Ossabaw Swine: A Preclinical Model of Cardio-Metabolic Heart Failure. *JACC Basic to Transl. Sci.* **4**, 404–421 (2019).

21. Torres, W. M. *et al.* Changes in Myocardial Microstructure and Mechanics With Progressive Left Ventricular Pressure Overload VISUAL ABSTRACT HIGHLIGHTS. *J Am Coll Cardiol Basic Trans Sci.* **5**, 463–80 (2020).

22. Singh, G. K. Congenital Aortic Valve Stenosis. *Children* **6**, 185–193 (2019).

23. Roberts, W. C. & Ko, J. M. Frequency by decades of unicuspid, bicuspid, and tricuspid aortic valves in adults having isolated aortic valve replacement for aortic stenosis, with or without associated aortic regurgitation. *Circulation* **111**, 920–925 (2005).

24. O'Brien, K. D. Epidemiology and genetics of calcific aortic valve disease. in *Journal of Investigative Medicine* vol. 55 284–291 (2007).

25. Brantley, H. P., Nekkanti, R., Anderson, C. A. & Kypson, A. P. Three-dimensional echocardiographic features of unicuspid aortic valve stenosis correlate with surgical findings. *Echocardiography* (2012) doi:10.1111/j.1540-8175.2012.01740.x.

26. Moller, J. H., Nakib, A., Eliot, R. S. & Edwards, J. E. Symptomatic congenital aortic stenosis in the first year of life. *J. Pediatr.* (1966) doi:10.1016/s0022-3476(66)80116-6.

27. Singh, S. *et al.* Unicuspid unicommissural aortic valve: An extremely rare congenital anomaly. *Texas Hear. Inst. J.* (2015) doi:10.14503/THIJ-13-3634.

28. Baillargeon, B., Rebelo, N., Fox, D. D., Taylor, R. L. & Kuhl, E. The living heart project: A robust and integrative simulator for human heart function. *Eur. J. Mech. A/Solids* **48**, 38–47 (2014).

29. Dassault Systèmes. SIMULIA Living Heart Human Model User Guide. (2017).

30. Rosalia, L., Ozturk, C., Van Story, D., Horvath, M. & Roche, E. T. Object-oriented lumped-parameter modelling of the cardiovascular system for physiological and pathophysiological conditions. *Adv. theory simulations* **4**, (2021).

31. Rosalia, L., Ozturk, C. & Roche, E. T. Lumped-Parameter and Finite Element Modeling of Heart Failure with Preserved Ejection Fraction. *J. Vis. Exp.* **168**, (2021).

32. Rajani, R., Hancock, J. & Chambers, J. B. The art of assessing aortic stenosis. *Heart* vol. 98 (2012).

33. Baumgartner, H. *et al.* Recommendations on the echocardiographic assessment of aortic valve stenosis: a focused update from the European Association of Cardiovascular Imaging and the American Society of Echocardiography. *Eur. Hear. journal. Cardiovasc. Imaging* **18**, 254–275 (2017).

34. Iung, B. *et al.* A prospective survey of patients with valvular heart disease in Europe: The Euro Heart Survey on valvular heart disease. *Eur. Heart J.* **24**, 1231–1243 (2003).

35. Mishra, S. & Kass, D. A. Cellular and molecular pathobiology of heart failure with preserved ejection fraction. *Nature Reviews Cardiology* 1–24 (2021) doi:10.1038/s41569-020-00480-6.

36. Pibarot, P. *et al.* Moderate Aortic Stenosis and Heart Failure With Reduced Ejection Fraction Can Imaging Guide Us to Therapy? (2019) doi:10.1016/j.jcmg.2018.10.021.

37. Azevedo, C. F. *et al.* Prognostic significance of myocardial fibrosis quantification by histopathology and magnetic resonance imaging in patients with severe aortic valve disease. *J. Am. Coll. Cardiol.* **56**, 278–287 (2010).

38. Goldsmith, E. C., Bradshaw, A. D. & Spinale, F. G. Cellular mechanisms of tissue fibrosis. 2. Contributory pathways leading to myocardial fibrosis: Moving beyond collagen expression. *Am. J. Physiol. - Cell Physiol.* **304**, (2013).

39. Zhu, Y. *et al.* Novel bicuspid aortic valve model with aortic regurgitation for hemodynamic status analysis using an ex vivo simulator. *J. Thorac. Cardiovasc. Surg.* **0**, (2020).

40. Genet, M., Lee, L. C., Baillargeon, B., Guccione, J. M. & Kuhl, E. Modeling Pathologies of Diastolic and Systolic Heart Failure. *Ann. Biomed. Eng.* **44**, 112–127 (2016).

41. Holman, D. M., Brionnaud, R. M. & Abiza, Z. *Solution to industry benchmark problems with the lattice-Boltzmann code Xflow*. *European Congress on Computational Methods in Applied Sciences and Engineering* (2012).

42. Ducros, F., Nicoud, F., Poinsot, T. & Dynamics, I. for C. F. *Wall-Adapting Local Eddy-Viscosity Models for Simulations in Complex Geometries*. (ICFD, Oxford University Computing Laboratory, 1998).

43. Mitchell, C. *et al.* Guidelines for Performing a Comprehensive Transthoracic Echocardiographic Examination in Adults: Recommendations from the American Society of Echocardiography. (2018) doi:10.1016/j.echo.2018.06.004.

44. Stypmann, J. *et al.* Echocardiographic assessment of global left ventricular function in mice. *Laboratory Animals* vol. 43 127–137 (2009).

Figures

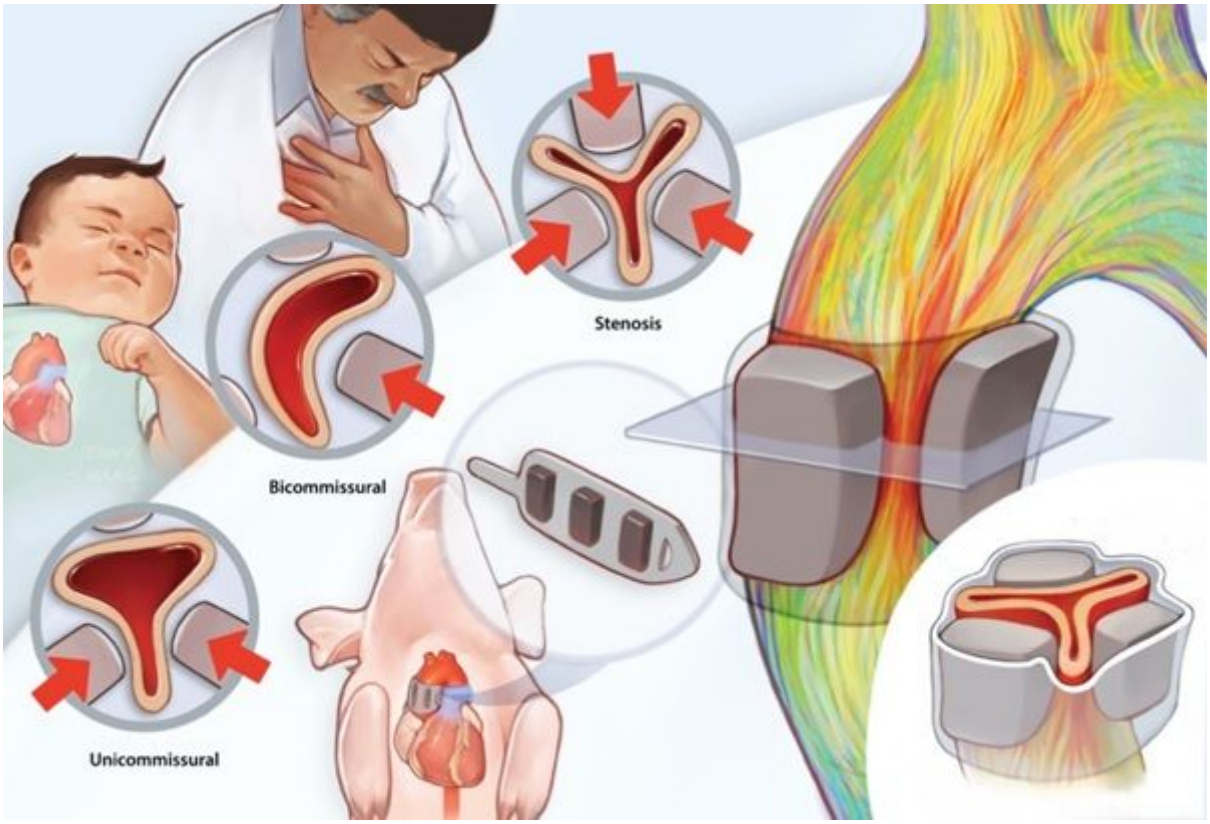

Figure 1

Overview of research impact. A high-fidelity in vivo model of aortic valve disease based on a bio-inspired soft robotic aortic sleeve. The tunability of the sleeve enables the recreation of the hemodynamics of

aortic stenosis (AS) and of congenital valve abnormalities, including those of bicommissural and unicommissural aortic valves, which arise from the fusion of one and two commissures respectively and are responsible for the accelerated onset and progression of AS. Magnetic Resonance Imaging allows visualization of the flow pattern induced by the soft robotic sleeve and hemodynamic mimicry of each valvular defect. By developing a high-fidelity animal model of aortic valve disease hemodynamics, this research is poised to profoundly impact the interventional paradigm for this condition. Illustration created by BioHues Digital.

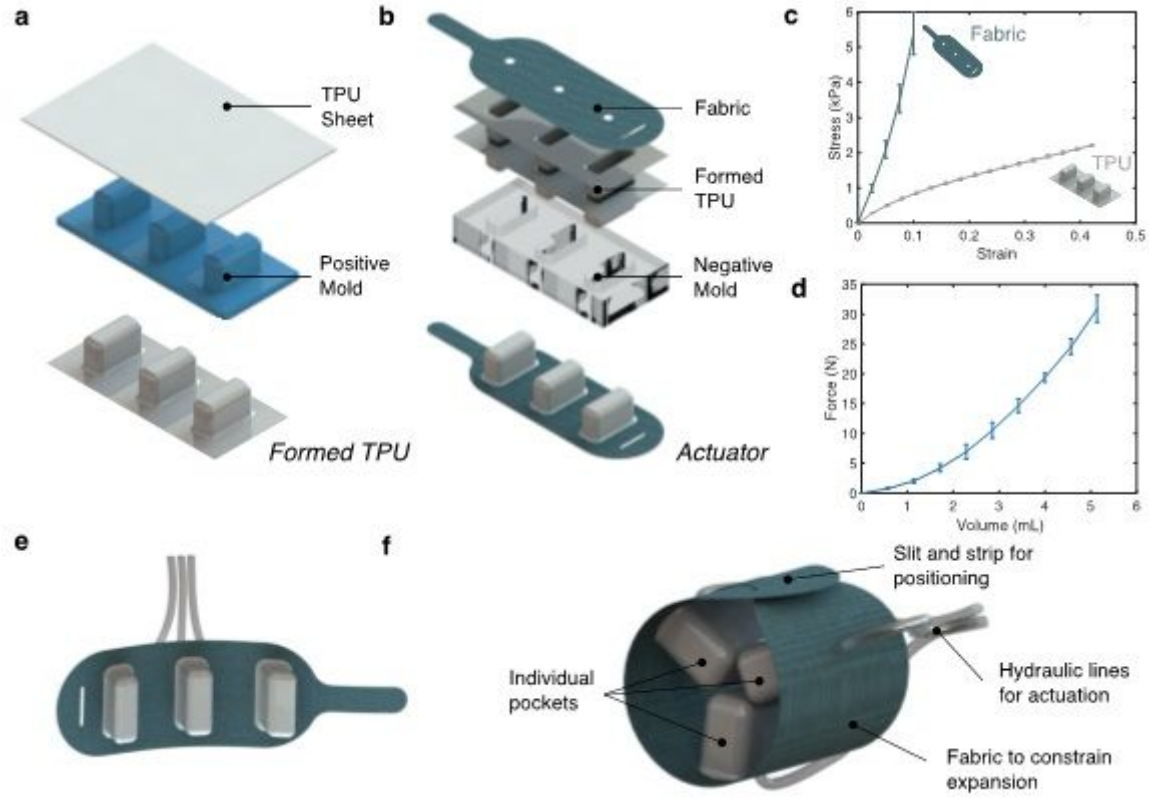

Figure 2

Design and manufacturing of the soft robotic aortic sleeve. a, Two thermoplastic polyurethane (TPU) sheets are vacuum formed to a positive 3D-printed mould. b, The two TPU sheets are then heat-sealed together creating three distinct expandable elements or pockets. They are then attached to a strain-limiting fabric thorough a heat-sealing process that utilizes a negative of the 3D-printed mould. c, Stress-strain response of the TPU and fabric layers under uniaxial tension. d, Axial force exerted by the sleeve at continuous actuation. e-f, 3D views of the aortic with details of the individual pockets, constraining fabric, hydraulic lines for actuation lines, and fabric slit and strip for positioning around the porcine ascending aorta. Data show mean ± SD, n = 3 for each data point.

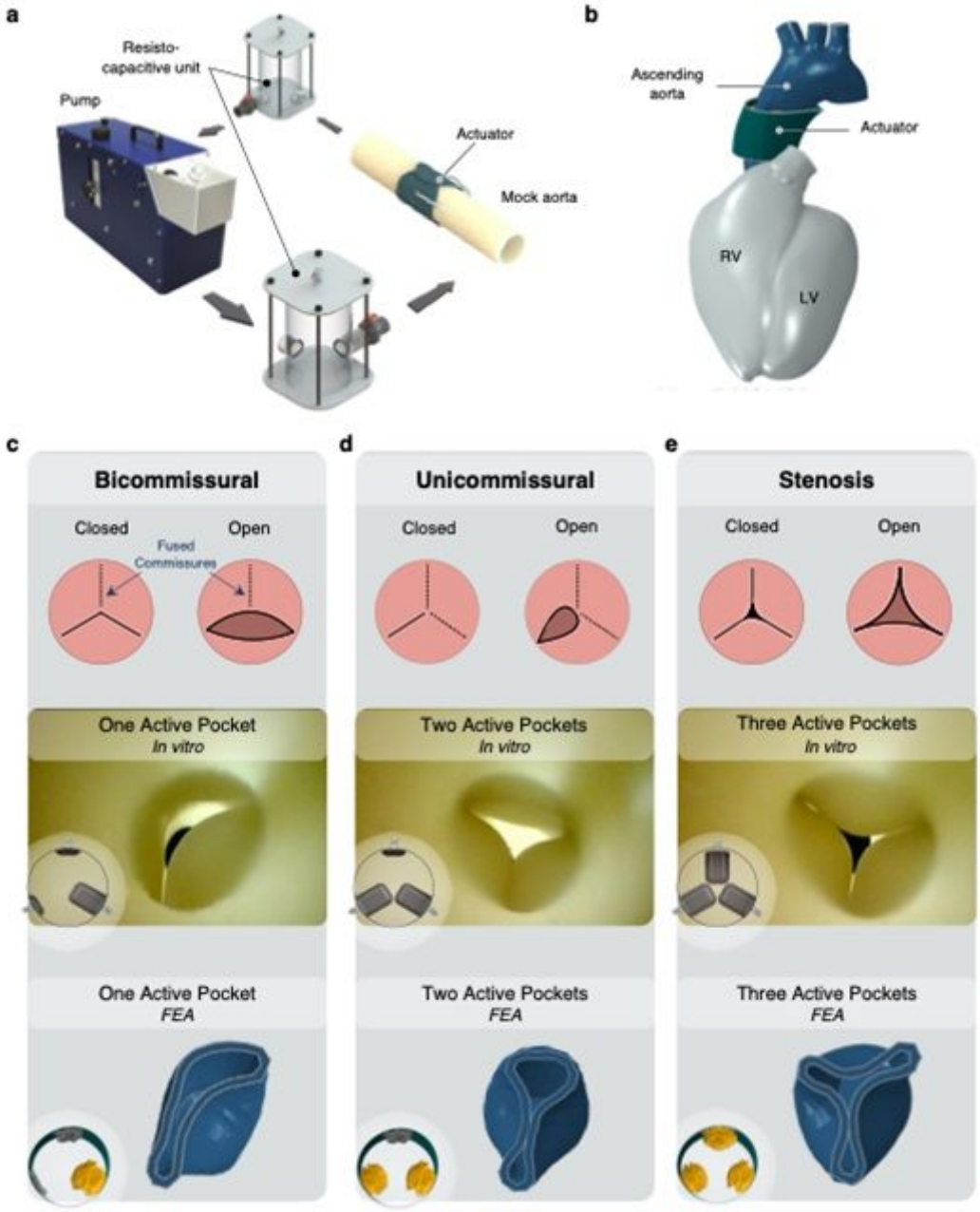

Figure 3

In vitro and in silico studies predict the luminal geometries of the ascending aorta following pocket-selective actuation. a, Illustration of the mock circulatory loop (MCL) composed of a pulsatile pump, two resisto-capacitive units, and a low-modulus tube to mimic the biomechanics of the ascending aorta. b, Living Heart finite element (FE) model including an accurate 3D representation of the soft robotic sleeve on the ascending aorta. c, Bicommissural, d, unicommissural and e, stenosis geometries of the anatomical valves in the closed and open configurations, and of the cross-sectional aortic profiles obtained on the MCL and predicted by FE, with illustrations of the actuated pockets of the sleeve for each profile.

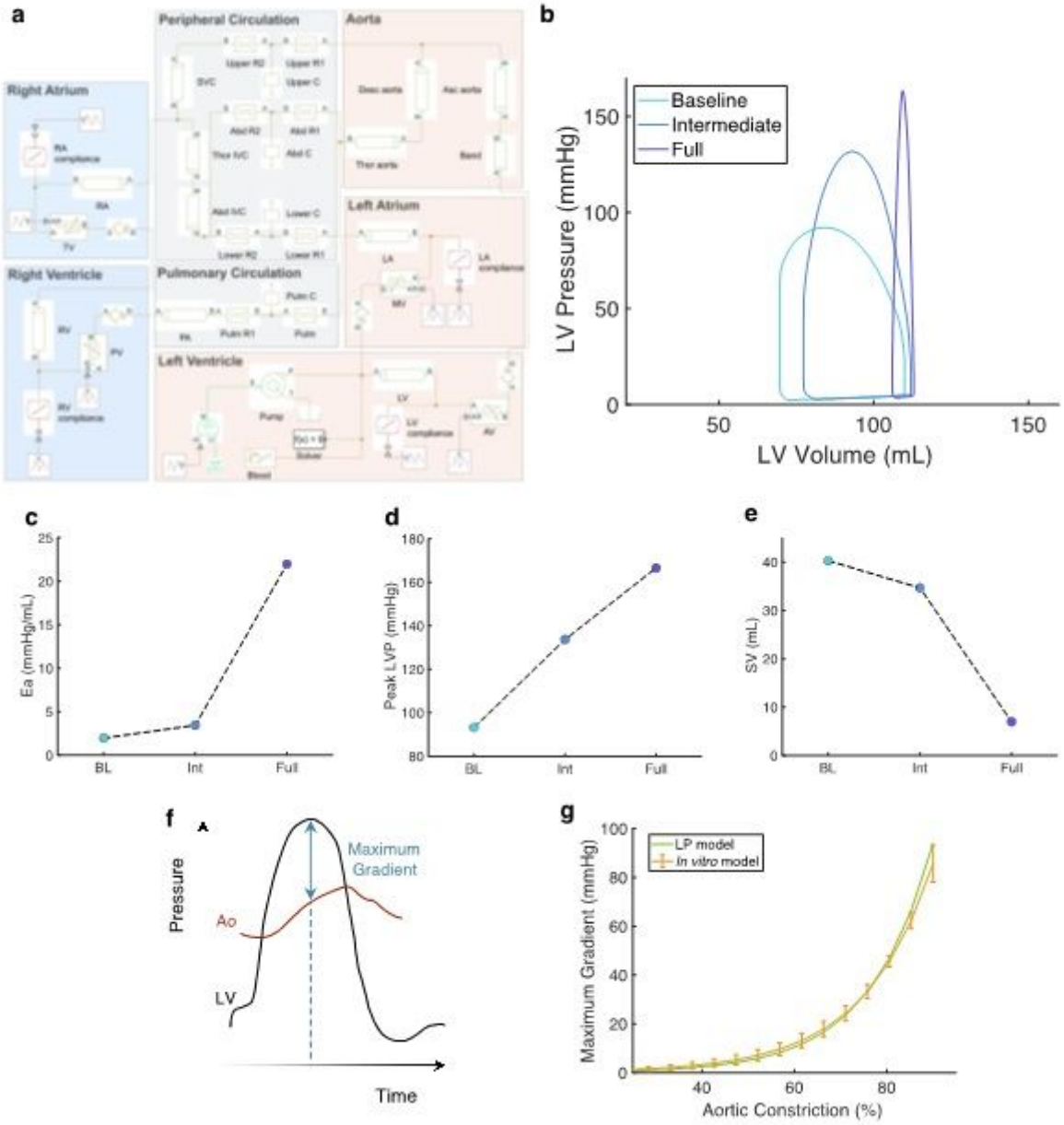

Figure 4

Hemodynamics of aortic constriction predicted by lumped-parameter modelling. a, Representation of the domain of the lumped-parameter (LP) model developed on SIMSCAPE FLUIDS and composed of a four-chamber heart, proximal vasculature, and peripheral and pulmonary circulations. b, Left ventricular (LV) pressure-volume (PV) loops obtained at baseline (BL), intermediate (Int: 80%) and full (Full: 90%) aortic constriction on the LP model, with corresponding, c arterial elastance (Ea), d peak left ventricular pressure (LVP), e stroke volume (SV) plots. f, Illustration of the LV and aortic (Ao) pressure waveforms during one heart cycle, highlighting the maximum transaortic pressure gradient. g, Maximum gradient versus percentage of luminal aortic constriction as predicted by LP and in vitro models. In vitro data show mean ± SD, n = 3 for each data point. Exponential regression was used for data fitting (LP: R2 = 0.9697; in vitro: R2 = 0.9958-0.9994).

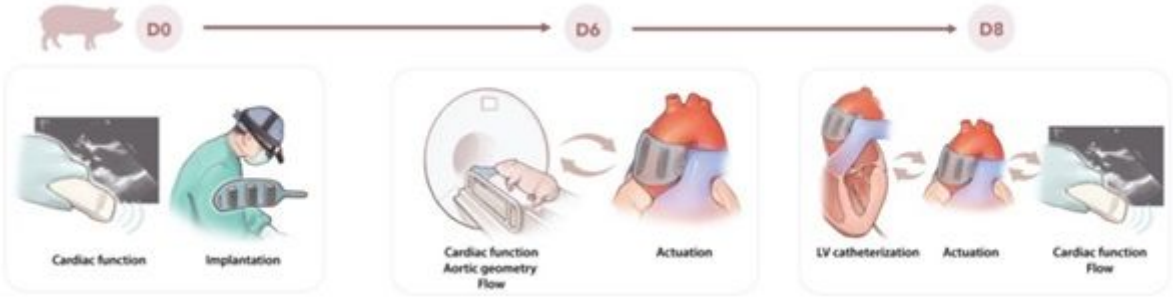

Figure 5

Timeline of in vivo studies. Metrics of cardiac function are assessed via transthoracic echocardiography (TTE) prior to implantation of the bio-inspired soft robotic aortic sleeve (D0). Six days post-surgery (D6), MRI studies are conducted to evaluate acute changes in cardiac function and aortic flow hemodynamics at various degrees of aortic constriction and actuation profiles. Eight days after implantation (D8), left ventricular (LV) catheterization and transepicardial echocardiography are performed following analogous actuation patterns to evaluate LV function and aortic flow. Illustration created by BioHues Digital.

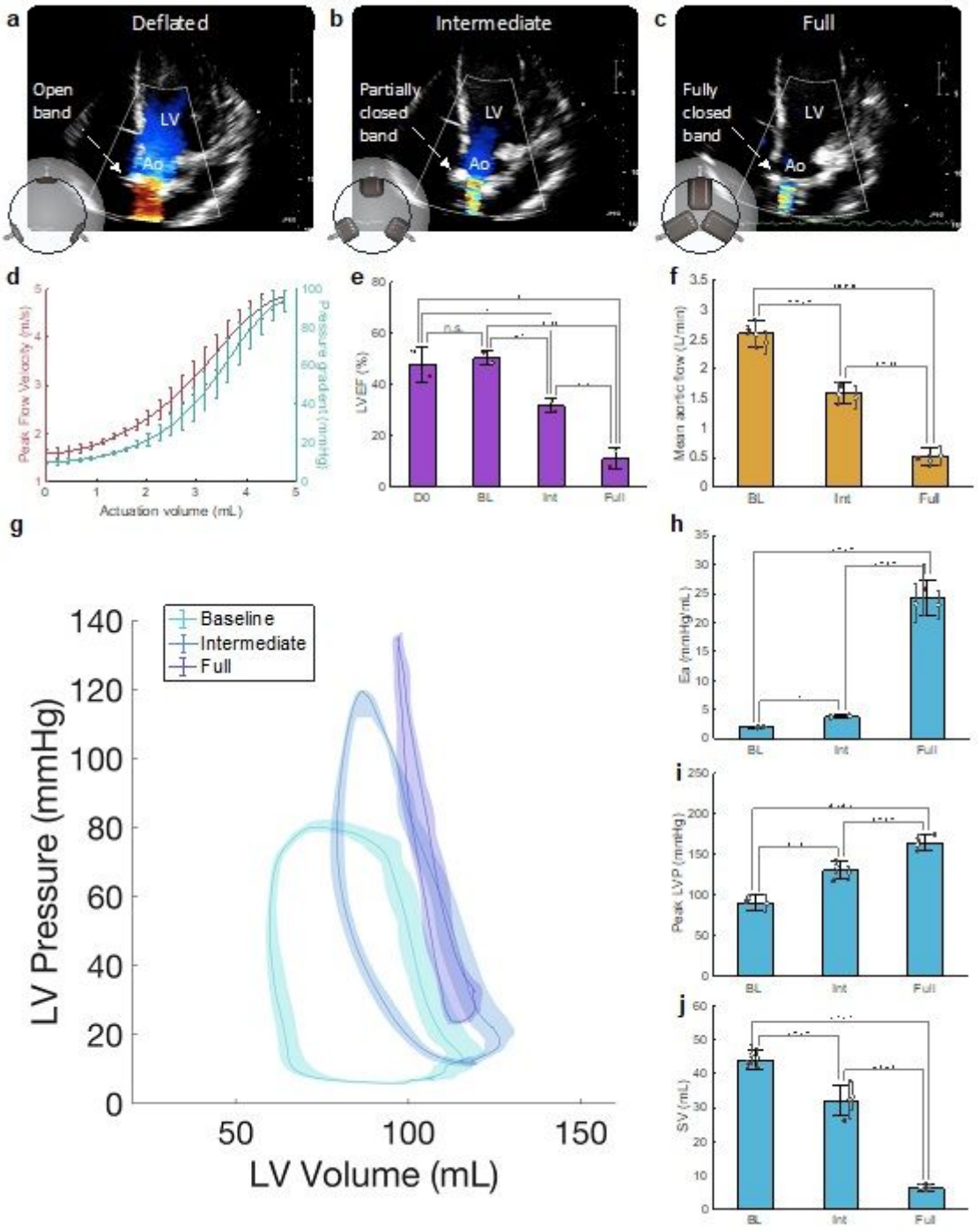

Figure 6

In vivo acute hemodynamic studies of the controllability of the bio-inspired soft robotic aortic sleeve. a-c, Transepicardial echocardiography colour Doppler images of blood flow during LV ejection (a) at baseline, (b) intermediate aortic constriction, and (c) full aortic constriction. d, Echocardiographic measurements of peak aortic flow velocity and corresponding estimates of maximum transaortic pressure gradient during continuous activation of the aortic sleeve from baseline to full constriction (n = 2). e, Measurements of left ventricular ejection fraction (LVEF) via transthoracic echocardiography (D0) before implantation surgery, and transepicardial echocardiography (D8) at baseline (BL), intermediate (Int) and full (Full) constriction (n = 2). f, Mean flow velocity measured at the thoracic aorta (n = 3). g, Representative left

ventricular (LV) pressure-volume (PV) loops at baseline, intermediate and full aortic constriction. Shaded area corresponds to mean ± SD of three consecutive heartbeats. h, Arterial elastance (Ea) measurements via LV catheterization (n = 3). i, Peak left ventricular pressure (LVP) measurements via LV catheterization (n = 3). j, Stroke volume (SV) measurements via LV catheterization (n = 3). In bar plots, large error bars represent 1 SD from the mean value across the animals, while smaller error bars show the SD within each animal averaged from 3 consecutive heart cycles. n.s: non-significant; *: P < 0.1, **: P < 0.05, ***: P < 0.01, ****: P < 0.001.

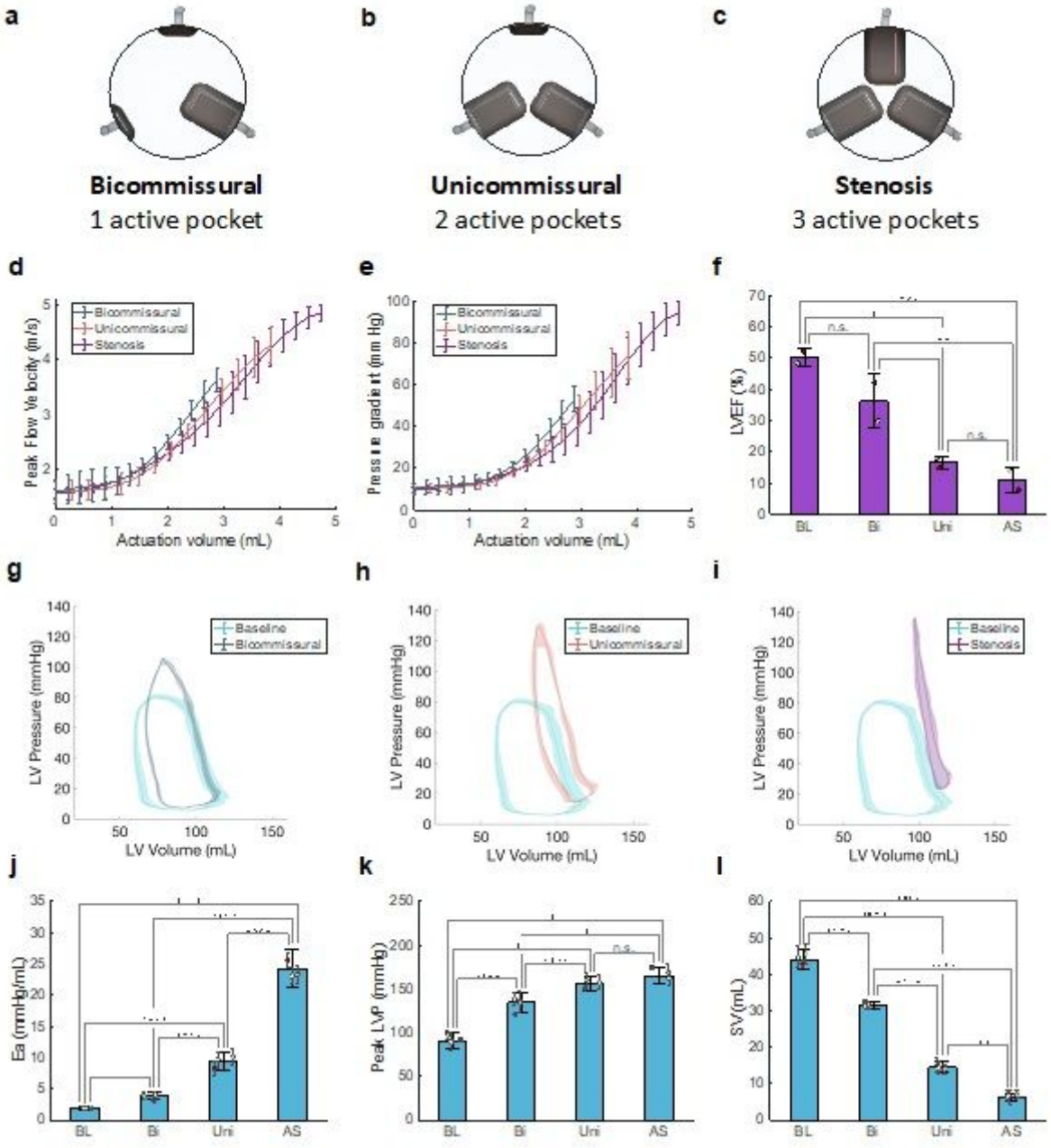

Figure 7

In vivo acute hemodynamic studies of the bicommissural, unicommissural, and aortic stenosis constriction profiles. a-c, Actuation patterns corresponding to the (a) bicommissural (Bi), (b) unicommissural (Uni), and (c) aortic stenosis (AS) profiles. d-f, Echocardiographic measurements of (d)

peak aortic flow velocity (n = 2), (e) corresponding estimates of maximum transaortic pressure gradient (n = 2), and (f) Left ventricular ejection fraction (LVEF) at baseline (BL) and during activation of the aortic sleeve for the various actuation profiles (n = 2). g-i, Representative left ventricular (LV) pressure-volume (PV) loops of the (g) bicommissural, (h) unicommissural, (i) stenosis profiles and comparison with baseline. Shaded area corresponds to mean ± SD of three consecutive heartbeats. j, Arterial elastance (Ea) measurements via LV catheterization (n = 3). k, Peak left ventricular pressure (LVP) measurements via LV catheterization (n = 3). l, Stroke volume (SV) measurements via LV catheterization (n = 3). In bar plots, large error bars represent 1 SD from the mean value across the animals, while smaller error bars show SD within each animal averaged from 3 consecutive heart cycles. n.s: non-significant; *: $P < 0.1$, **: $P < 0.05$, ***: $P < 0.01$, ****: $P < 0.001$.

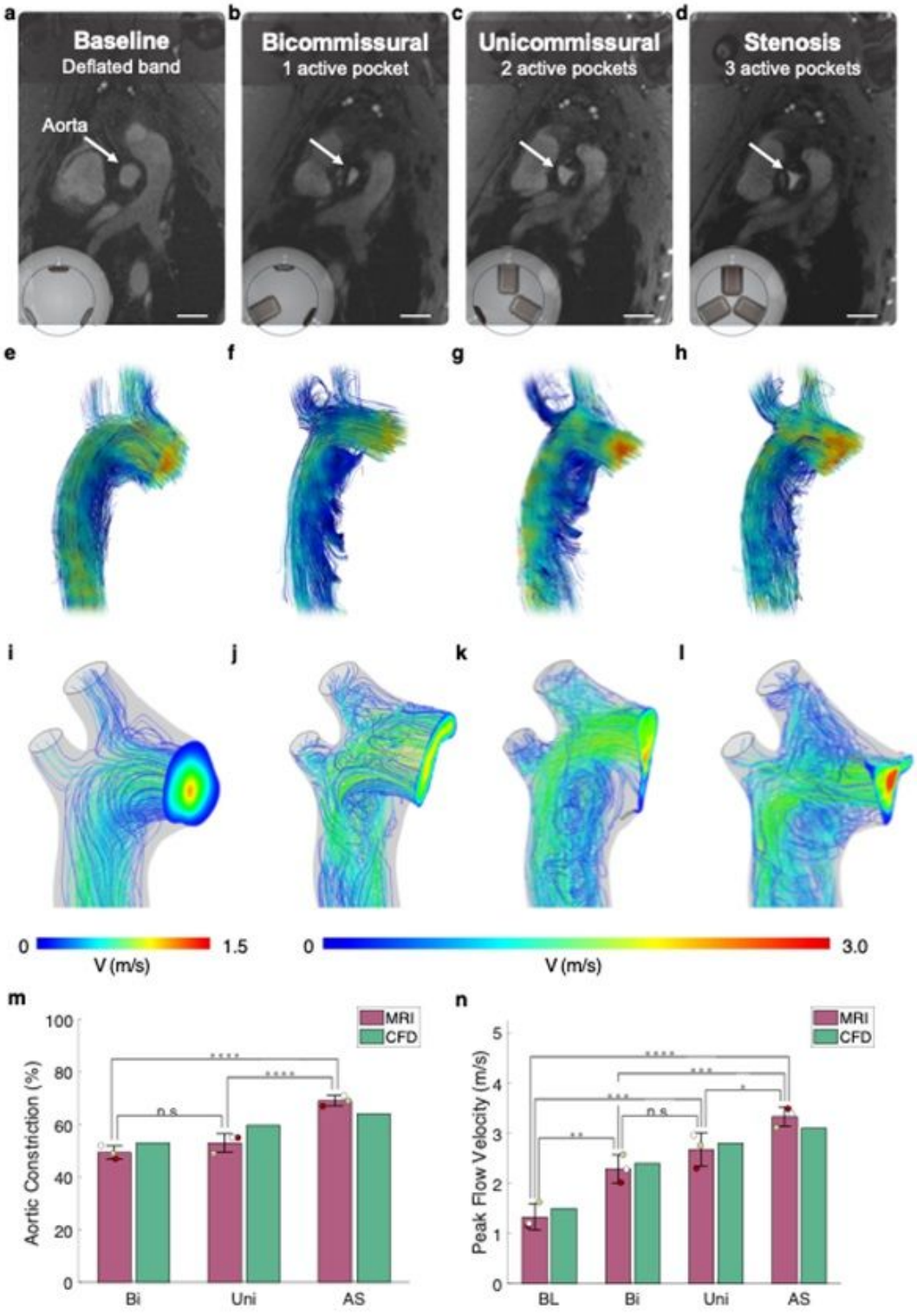

Figure 8

In vivo and CFD aortic flow hemodynamics of the bicommissural, unicommissural, and aortic stenosis constriction profiles. a-d, Representative 2D CINE-MRI cross-sectional views of the aorta at (a) baseline (BL), and for the (b) bicommissural (Bi), (c) unicommissural (Uni), and (d) aortic stenosis (AS) profiles in vivo. Scale bars, 2 cm. e-h, Representative aortic flow obtained using 4D- at (e) baseline, and for the (f) bicommissural, (g) unicommissural, and (h) stenosis profiles in vivo. i-l, Aortic streamlines obtained by

the computational fluid dynamics (CFD) model at (i) baseline, and for the (j) bicommissural, (k) unicommissural, and (l) stenosis profiles. Velocity boundaries are homogeneous for e and i and for f-h and j-l. m, Comparison of aortic constriction calculated as percentage change of aortic cross-sectional area for the three actuation patterns between MRI study (n = 3) and CFD model. n, Comparison of peak aortic flow velocity between MRI study (n = 3) and CFD model. n.s: non-significant; *: P < 0.1, **: P < 0.05, ***: P < 0.01, ****: P < 0.001.

Supplementary Files

This is a list of supplementary files associated with this preprint. Click to download.

- NBMESIRosalia.docx
- LRVS1compressed.mp4
- LRVS2.mp4
- LRVS3compressed.mp4
- LRVS4.mp4
- SupplementaryInformation.pdf